

32. N. M. Stano, S. S. Patel, *J. Mol. Biol.* **315**, 1009 (2002).
33. L. G. Briebe, R. Sousa, *Biochemistry* **40**, 3882 (2001).
34. P. A. Bullough, F. M. Hughson, J. J. Skehel, D. C. Wiley, *Nature* **371**, 37 (1994).
35. J. Kuriyan, M. O'Donnell, *J. Mol. Biol.* **234**, 915 (1993).
36. V. A. Bloomfield, D. M. Crothers, I. Tinoco Jr., *Nucleic Acids: Structures, Properties, and Functions* (University Science Books, Sausalito, CA, 2000).
37. F. M. Richards, *Annu. Rev. Biophys. Bioeng.* **6**, 151 (1977).
38. G. A. Diaz, M. Rong, W. T. McAllister, R. K. Durbin, *Biochemistry* **35**, 10837 (1996).
39. Y. Jia, A. Kumar, S. S. Patel, *J. Biol. Chem.* **271**, 30451 (1996).
40. A. Ujvari, C. T. Martin, *J. Mol. Biol.* **273**, 775 (1997).
41. V. Gopal, L. G. Briebe, R. Guajardo, W. T. McAllister, R. Sousa, *J. Mol. Biol.* **290**, 411 (1999).
42. P. S. Freemont, J. M. Friedman, L. S. Beese, M. R. Sanderson, T. A. Steitz, *Proc. Natl. Acad. Sci. U.S.A.* **85**, 8924 (1988).
43. S. Doublié, S. Tabor, A. M. Long, C. C. Richardson, T. Ellenberger, *Nature* **391**, 251 (1998).
44. _____, T. Ellenberger, *Curr. Opin. Struct. Biol.* **8**, 704 (1998).
45. A. Kornberg, T. Baker, *DNA Replication* (Freeman, New York, ed. 2, 1991).
46. U. K. Urs, R. Murali, H. M. Krishna Murthy, *Acta Crystallogr.* **D 55**, 1971 (1999).
47. J. Huang, J. Villemain, R. Padilla, R. Sousa, *J. Mol. Biol.* **293**, 457 (1999).
48. A. Kumar, S. S. Patel, *Biochemistry* **36**, 13954 (1997).
49. A. L. Gnat, P. Cramer, J. Fu, D. A. Bushnell, R. D. Kornberg, *Science* **292**, 1876 (2001).
50. P. Cramer, D. A. Bushnell, R. D. Kornberg, *Science* **292**, 1863 (2001).
51. M. C. Franklin, J. Wang, T. A. Steitz, *Cell* **105**, 657 (2001).
52. K. S. Murakami, S. Masuda, E. A. Campbell, O. Muzzin, S. A. Darst, *Science* **296**, 1285 (2002).
53. D. G. Vassilyev *et al.*, *Nature* **417**, 712 (2002).
54. S. S. Daube, P. H. von Hippel, *Proc. Natl. Acad. Sci. U.S.A.* **96**, 8390 (1999).
55. S. Doublié, in *Methods in Enzymology*, C. W. Carter and R. M. Sweet, Eds. (Academic Press, San Diego, CA, 1997), vol. 277, pp. 523–530.
56. Z. Otwinowski, W. Minor, in *Methods in Enzymology* C. W. Carter and R. M. Sweet, Eds. (Academic Press, San Diego, CA 1997), vol. 277, pp. 307–326.
57. M. Navarro, G. A. Cross, E. Wirtz, *EMBO J.* **18**, 2265 (1999).
58. A. T. Brünger *et al.*, *Acta Crystallogr.* **D54**, 905 (1998).
59. J. A. Christopher, SPOCK: The Structural Properties Observation and Calculation Kit (Program Manual) (The Center for Macromolecular Design, Texas A&M University, College Station, TX, 1998).
60. M. Carson, in *Methods in Enzymology*, C. W. Carter and R. M. Sweet, Eds. (Academic Press, San Diego, CA, 1997), vol. 277, pp. 493–505.
61. Data were collected at two synchrotron sources for this work, ID-19 at Argonne National Labs (APS) and X25 at National Synchrotron Light Source (NSLS). Use of the Argonne National Laboratory Structural Biology Center beamlines at the Advanced Photon Source was supported by the U.S. Department of Energy (DOE), Office of Biological and Environmental Research, under Contract No. W-31-109-ENG-38. Research carried out in part at the NSLS, BNL, was supported by the DOE, Division of Materials Sciences and Division of Chemical Sciences, under Contract No. DE-AC02-98CH10886. We thank M. Becker (X25) and A. Joachimiak (ID-19) for their support during beamline data collections; W. Kennedy, C. Joyce, and S. Kamtekar for many helpful discussions and critical reading of the manuscript; and D. Crothers for help with the thermodynamic calculations. The coordinates for the T7 RNAP elongation complex have been deposited in the PDB under accession code 1msw. Supported by NIH grant GM57510 to T.A.S.

16 August 2002; accepted 11 September 2002

Published online 19 September 2002;

10.1126/science.1077464

Include this information when citing this paper.

Projection of an Immunological Self Shadow Within the Thymus by the Aire Protein

Mark S. Anderson,¹ Emily S. Venanzi,¹ Ludger Klein,² Zhibin Chen,¹ Stuart P. Berzins,¹ Shannon J. Turley,¹ Harald von Boehmer,² Roderick Bronson,³ Andrée Dierich,⁴ Christophe Benoist,^{1*} Diane Mathis^{1*}

Humans expressing a defective form of the transcription factor AIRE (autoimmune regulator) develop multiorgan autoimmune disease. We used *aire*-deficient mice to test the hypothesis that this transcription factor regulates autoimmunity by promoting the ectopic expression of peripheral tissue-restricted antigens in medullary epithelial cells of the thymus. This hypothesis proved correct. The mutant animals exhibited a defined profile of autoimmune diseases that depended on the absence of *aire* in stromal cells of the thymus. Aire-deficient thymic medullary epithelial cells showed a specific reduction in ectopic transcription of genes encoding peripheral antigens. These findings highlight the importance of thymically imposed "central" tolerance in controlling autoimmunity.

A problem that has intrigued immunologists for decades is how animals achieve immunological tolerance to autoantigens (1). For example, T cells are generated in the thymus,

and because their antigen-specific receptors are encoded by genes assembled through random somatic DNA rearrangement, the emergent repertoire of receptors inevitably includes specificities capable of reacting to self constituents. To avoid the potentially pathological state of autoimmunity, it is necessary to purge these self-reactive cells from the repertoire, either by removal or silencing. Some are removed in the thymus soon after generation, but this raises the question of how thymocytes that are reactive to proteins expressed only in nonthymic parenchymal tissues can be identified and dealt with. A commonly held notion involves a dichotomy of "central" and "peripheral" mechanisms: Tol-

erance to ubiquitously expressed or blood-borne antigens is achieved in the thymus, whereas tolerance to tissue-restricted antigens is secured by means of diverse extrathymic processes.

Surprisingly, RNA transcripts encoding a multiplicity of proteins previously considered to be synthesized only in particular peripheral tissues can be detected in the thymus (2, 3), specifically in very rare epithelial cells in the medulla (4, 5). Examples include transcripts encoding transcription factors, structural proteins, membrane proteins, hormones, and secreted proteins. Thymic medullary epithelial cells (MECs) have been increasingly implicated in the clonal deletion or inactivation of semi-mature self-reactive thymocytes (6, 7), fueling interest in the precise function of these ectopically expressed transcripts. Several transgenic (4, 8–17) and nontransgenic (18, 19) mouse systems have revealed a direct link between ectopic synthesis of a designated protein in MECs and the absence of peripheral lymphocyte reactivity to that protein. Many of the ectopically expressed antigens (insulin, thyroglobulin, myelin basic protein, and retinal S-antigen) are associated with organ-specific autoimmune diseases (type 1 diabetes, thyroiditis, multiple sclerosis, and uveitis, respectively). In addition, there are some very suggestive correlations between antigen expression levels in the thymus and disease susceptibility in humans (20, 21) and rodents (22). We sought to determine what drives ectopic synthesis of peripheral tissue-restricted proteins in MECs, and what impact this expression has on an animal's state of immunological self tolerance.

Following clues from the human system, we anticipated that mice lacking the *aire* gene would prove key to addressing these issues. Autoimmune polyendocrinopathy–candidia-

¹Section on Immunology and Immunogenetics, Joslin Diabetes Center; Department of Medicine, Brigham and Women's Hospital; Harvard Medical School, 1 Joslin Place, Boston, MA 02215, USA. ²Dana Farber Cancer Institute, 44 Binney Street, Boston, MA 02115, USA. ³Harvard Medical School, 200 Longwood Avenue, Boston, MA 02115, USA. ⁴Institut de Génétique et de Biologie Moléculaire et Cellulaire, CNRS/INSERM/ULP, 1 rue Laurent Fries, 67404 Strasbourg, France.

*To whom correspondence should be addressed. E-mail: cbdm@joslin.harvard.edu

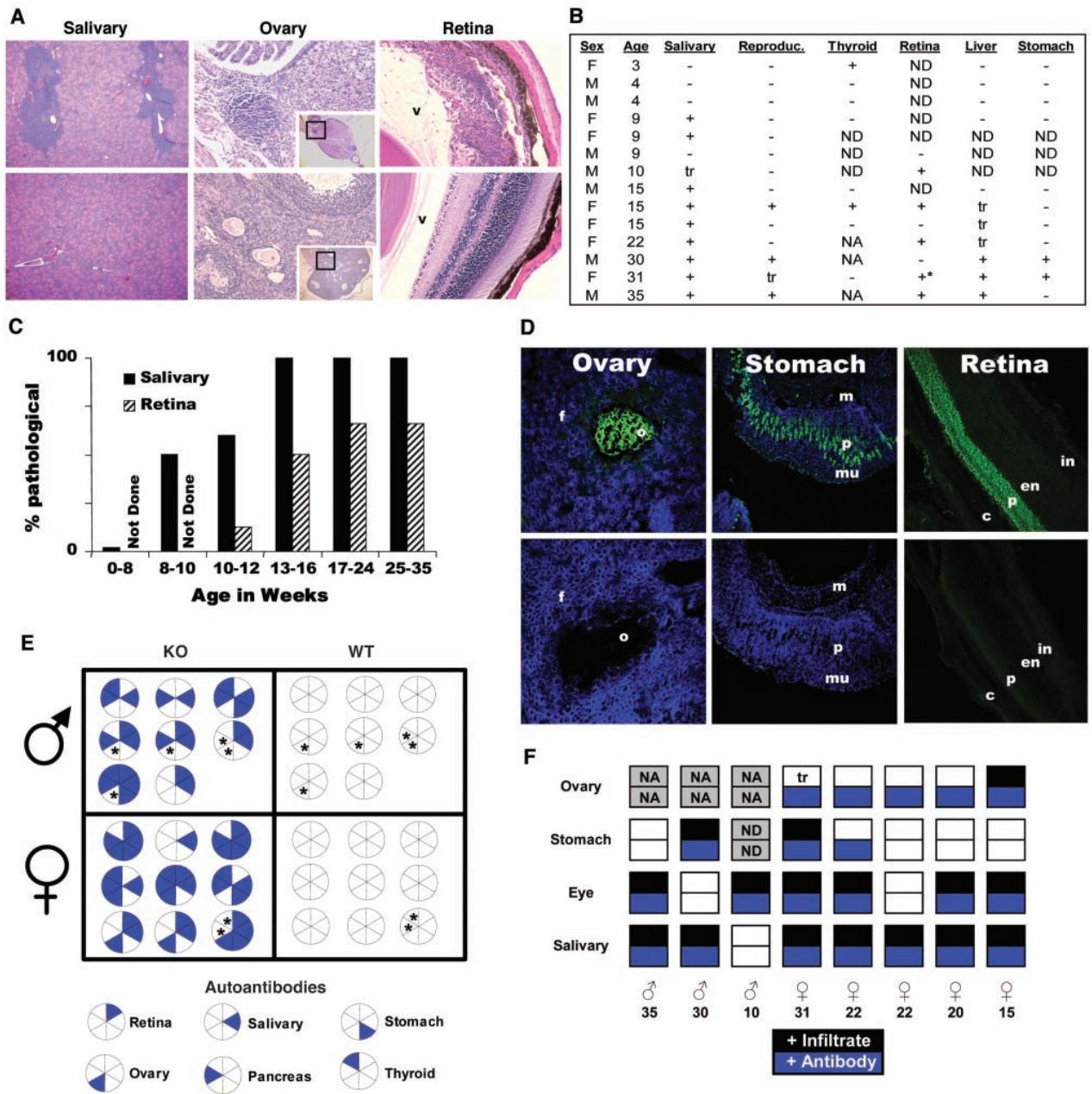


Fig. 1. Aire-deficient mice develop autoimmunity. **(A)** Tissue sections from aire-deficient mice from salivary gland (magnification $\times 50$, 35-week-old males), ovary ($\times 200$, inset $\times 50$ with area of $\times 200$ view highlighted, 15-week-old females), and retina ($\times 200$, 31-week-old females; v, vitreous) from aire-deficient (i.e., knockout; top row) and wild-type (bottom row) mice stained with hematoxylin and eosin (H&E). Each knockout section shows representative lymphocytic infiltrates. **(B)** Table summarizes presence (+) or absence (-) of lymphocytic infiltrates observed in knockout mice of various ages and both sexes for the indicated organs. "Reproduc." refers to ovaries in female mice and to the coagulating glands in male mice. For the retina, many mice had retinal degeneration and were scored +; in addition, one mouse had retinal degeneration with immune infiltration and is scored +*. NA, not available; ND, not done; tr, trace infiltrate. Age- and sex-matched wild-type mice were also examined, and no infiltrate was seen in any mouse in any of the indicated organs ($n = 14$). **(C)** Salivary gland infiltrates and retinal degeneration develop in a time-dependent manner. Shown are percentages of mice with salivary gland infiltrates or retinal degeneration killed at the given age ranges; $n = 21$ for the salivary gland and $n = 16$ for the retina. **(D)** Aire-deficient mice have autoantibodies to multiple organs. Shown is representative

staining by indirect immunofluorescence on tissue sections of ovary (magnification $\times 250$), stomach ($\times 100$), and retina ($\times 250$) for serum from individual knockout (top row) or age- and sex-matched wild-type (bottom row) mice. Green indicates serum staining; blue indicates staining with the nuclear marker 4',6'-diamidino-2-phenylindole (DAPI) (not done on retina sections). For the ovary, knockout serum reacted against the cytoplasm of the oocyte (marked o; f, follicle). For the stomach, knockout serum stained the parietal cell layer (marked p; mu, mucinous layer; m, muscular layer). The retinal staining revealed knockout serum that reacted against the outer retinal layer containing the epithelium and rods and cones (marked p; c, choroid; en, external nuclear layer; in, inner nuclear layer). **(E)** Summary of autoantibodies in aire-deficient mice. Serum from age- and sex-matched mice (9 to 35 weeks old) was collected and tested for the presence of autoantibodies to the indicated organs. Each circle represents an individual mouse, with the corresponding autoantibody indicated by the key below the chart; *, not done. **(F)** Summary of correlation of autoantibodies to immune infiltrates for ovary, salivary gland, retina, and stomach in seven knockout mice. For each mouse of the indicated sex and age (in weeks), detection of an infiltrate or an autoantibody is indicated. NA, not available; ND, not done; tr, trace infiltrate.

sis–ectodermal dystrophy (APECED), also known as autoimmune polyendocrine syndrome–type 1 (APS-1), is a polyglandular disorder that classically manifests as spontaneous autoimmunity against the parathyroid and/or adrenal glands, and/or by a mucocutaneous candidiasis infection [reviewed in (23, 24)]. Other common ailments include autoimmune forms of premature ovarian failure, hepatitis, anemia, diabetes, alopecia, and vitiligo. Disease is inherited in an autosomal recessive manner as a result of loss of function of a single susceptibility gene, which encodes the AIRE protein. AIRE has shown DNA binding activity (25) and transcriptional transactivation potential (26, 27) in assays in vitro. This protein and its murine homolog, *aire*, have a pattern of expression that suggests a potential role in shaping the T cell

repertoire: By far the highest amounts are found in the thymus, specifically in MECs (4, 28, 29). It seemed reasonable to hypothesize that APECED patients develop multiorgan autoimmunity because a defect in AIRE prevents or modifies ectopic transcription of genes encoding peripheral tissue–restricted antigens in thymic MECs. A recent report that *aire*-deficient mice also exhibit autoimmune manifestations is consistent with this proposal, although that study concluded that the cause was a problem with peripheral lymphocyte homeostasis (30). Here, we investigated an independently generated line of *aire*-deficient mice in an effort to learn whether the spectrum of autoimmunity manifested by these mice is consistent with a broad defect in central tolerance induction, and whether this results from an alteration in ectopic expres-

sion of tissue-restricted antigens by thymic MECs.

We engineered a line of mice carrying a defective *aire* gene by means of *lox/cre*-mediated recombination in embryonic stem (ES) cells (fig. S1). These mice carry in homozygous state a mutant allele bearing a deletion of exon 2 and portions of the upstream and downstream introns (fig. S1A). Mature *aire* gene transcripts could be detected at near-normal levels in the thymus of mutant mice, but these were smaller than in the wild type, as expected given the absence of exon 2 (fig. S1B). Sequence analysis confirmed that these transcripts could not give rise to functional protein because a frame shift provoked by the abnormal juxtaposition of exons 1 and 3 resulted in premature truncation shortly after exon 1 (fig. S1C). The *aire* gene mutation was generated in ES cells derived from mice of the Sv/129 strain, and mice used in the experiments described here were from F₂ or F₃ backcrosses onto the B6 genetic background.

Aire prevents autoimmunity. We first tested whether the absence of *aire* in these mice leads to broad defects in tolerance induction. Lymphocyte infiltrates were observed in several organs, usually confined to particular structures rather than being distributed indiscriminately throughout the organ. For example, lymphocytes were seen in the salivary gland only in the perivascular regions, in the ovary only in the follicles, and in the eye only in the retina (Fig. 1A). The infiltrates showed a pronounced age dependence by two criteria: (i) The number of organs targeted increased in older *aire*-deficient mice, ranging from none or one at 3 to 4 weeks of age to at least four or five after 30 weeks (Fig. 1B). (ii) For any particular organ, the fraction of mutant mice with autoimmune manifestations increased with age. For example, salivary gland infiltrates were rare in mice less than 8 weeks of age but were constant after 13 weeks (Fig. 1C). Autoantibodies had the same kind of target distribution. Multiple organs were targeted, but only at specific substructures within each (e.g., oocytes in the ovary, parietal cells in the stomach, the outer layer of the retina in the eye). All *aire*-deficient mice had serum autoantibodies after 3 to 6 months of age, most with reactivity to several organs, as detected by staining of tissues from wild-type mice (Fig. 1D). In the majority of *aire*-deficient mice, there was a good correlation between organs targeted by infiltrates and those targeted by autoantibodies (Fig. 1F). In short, the phenotype of these *aire*-deficient mice is certainly compatible with a broad defect in tolerance induction, but one characterized by highly selective, rather than indiscriminate, autoimmune attack.

We next sought to determine whether the

Fig. 2. Flow cytometric analysis of lymphoid organs in *aire*-deficient mice. (A) Increased number of thymic MECs in knockout mice. Pooled thymic stromal cells from five knockout (KO) or wild-type (WT) mice were stained with anti-CD45, CDR1, G8.8, and anti-B7-1. The plots contain only the CD45⁺G8.8⁺ cells. Cortical epithelial cells are CDR1^{hi}B7-1^{lo}, and MECs (circled) are CDR1^{int}B7-1^{hi}. Numbers ($\times 10^5$) of cells in each gate are shown from one of four representative experiments. (B) Increased activation/memory markers in *aire*-deficient T cells. Cells from peripheral lymph nodes of individual mice were isolated and stained. Shown are representative plots for a wild-type and a knockout mouse with CD4⁺ cells gated on the left and activation markers CD44 and CD62L on the right. The percentages of CD4⁺ cells that are CD44^{hi}CD62L^{lo} for a representative knockout and wild-type mouse are indicated. The ratio of the knockout CD44^{hi}CD62L^{lo} percentage versus the wild-type CD44^{hi}CD62L^{lo} percentage for CD4⁺ cells from 10 knockout and 9 wild-type mice 3 to 15 weeks of age is also indicated. A similar increase in CD44^{hi}CD62L^{lo} cells was also seen for CD8⁺ cells (32).

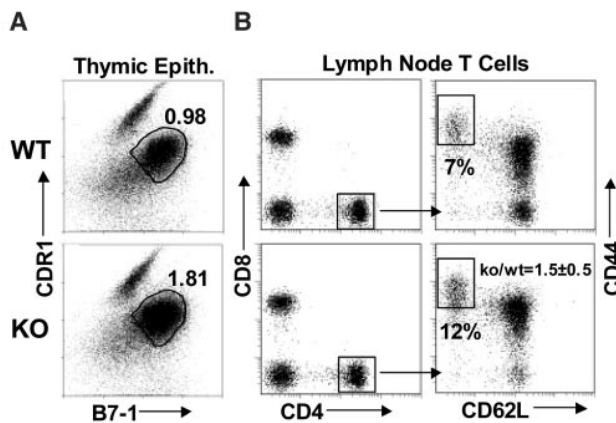
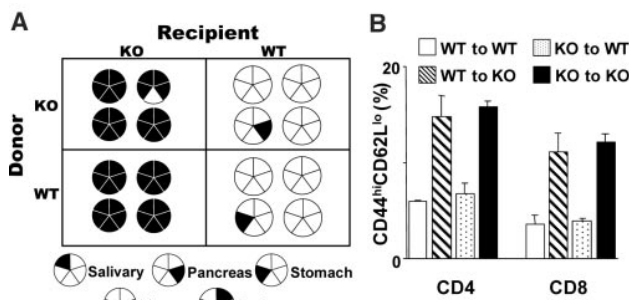


Fig. 3. Absence of *aire* in stromal cells leads to autoimmunity. (A) Bone marrow from knockout or wild-type mice was transferred into lethally irradiated recipient knockout or wild-type mice in a classic crisscross fashion, yielding four experimental groups. Organs were harvested 2 months after reconstitution and analyzed for autoimmunity. The circles represent individual mice and summarize the pattern of immune infiltrates from 16 mice (four from each group) in the indicated organs (see fig. S8 for representative H&E stains). Autoantibodies were also detected for stomach, salivary gland, pancreas, liver, and retina; these followed an identical pattern to the infiltrate data and are not shown separately. (B) Analysis of activation markers on CD4⁺ and CD8⁺ T cells from bone marrow chimeras. Inguinal lymph nodes were harvested and analyzed by flow cytometry for CD4, CD8, CD44, and CD62L. Data represent four mice in each group in two experiments. T cells from spleens, cervical lymph nodes, mesenteric lymph nodes, and pancreatic lymph nodes exhibit similar patterns (32).



autoimmunity exhibited by aire-deficient mice was reflected in other immune system abnormalities. Most of the features examined histologically, cytofluorimetrically, or via functional assays appeared within the normal range (31) (figs. S2 to S7), in general agreement with previous findings (30). These included thymocyte numbers, CD4/CD8 subset distributions, and differentiation marker profiles; bone marrow cell numbers and immunoglobulin M (IgM)/B220 profiles; spleen and lymph node cell numbers, IgM/TCR (T cell receptor)- $\alpha\beta$, IgM/IgD, and CD4/CD8 profiles and

CD4⁺CD25⁺ regulatory T cell compartments; dendritic cell numbers and subsets; T cell cytokine production after anti-CD3/CD28 stimulation; in vitro presentation of antigens or peptides; stimulatory and response capacity in mixed lymphocyte reactions; and thymus, spleen, and lymph node histology. Two features of the immune system in mutant mice were abnormal, however. There was an average doubling of the number of MECs (Fig. 2A), although expression of major histocompatibility complex (MHC) class II and costimulatory molecules were normal (32) and there was a

near-doubling in the frequency of activated/memory CD44^{hi}CD62L^{lo} T cells in both the CD4⁺ and CD8⁺ compartments of the peripheral lymphoid organs of most mice (Fig. 2B). This latter observation is consistent with the possibility that aire somehow functions to reduce the self reactivity of peripheral T cells.

Requirement for aire expression in the thymic stroma. To establish whether the autoimmune manifestations in aire-deficient mice are attributable to its absence from radioresistant or hematopoietic cells, we constructed a set of radiation bone marrow chimeras, which produced aire in radioresistant cells only, in hematopoietic cells only, in neither cell type, or in both. Signs of autoimmunity were detected only in those chimeras that lacked aire in the radioresistant cells. Lymphocytic infiltrates were found in all irradiated aire-deficient recipients, whether the donors of bone marrow cell precursors expressed aire or not. The invasiveness of the infiltrates was strikingly enhanced in these chimeras vis-à-vis unmanipulated mutant mice according to multiple criteria: the fraction of young mice showing infiltrates, number of organs infiltrated, and extent of the infiltrate (Fig. 3A) (fig. S8). Likewise, irradiated aire-deficient recipients of both wild-type and mutant bone marrow cell precursors exhibited serum autoantibodies, and these were more prevalent and had a wider target range than was found with unmanipulated mutant mice (Fig. 3A). Again, the profiles of organs targeted by infiltrates and by autoantibodies were closely correlated (Fig. 3A). Finally, the abnormal accumulation of activated/memory CD44^{hi}CD62^{lo} cells, both CD4⁺ and CD8⁺, also correlated with the absence of aire in radioresistant cells (Fig. 3B). Thus, the autoimmune manifestations in aire-deficient mice reflect this protein's function in radioresistant cells.

The next issue to resolve was whether aire exerts its influence on autoimmunity within the thymus or the periphery. Although aire and its human equivalent are predominantly synthesized in the thymus, expression in a number of peripheral tissues has also been reported, including several of those targeted by lymphocytic infiltrates or autoantibodies in aire-deficient individuals (33, 34). However, expression in peripheral parenchymal tissues has been controversial (35, 36), primarily because of its weakness and irreproducibility (35, 36). We carefully examined *aire* gene expression in normal mice by quantitative real-time polymerase chain reaction (PCR) (Fig. 4A). Transcripts were by far the most abundant in the thymus. Although transcripts were also detected in peripheral lymphoid organs (at significantly lower levels), they were essentially undetectable in the parenchymal tissues examined other than the ovary. These results imply that target tissues need not synthesize significant levels of aire to avoid

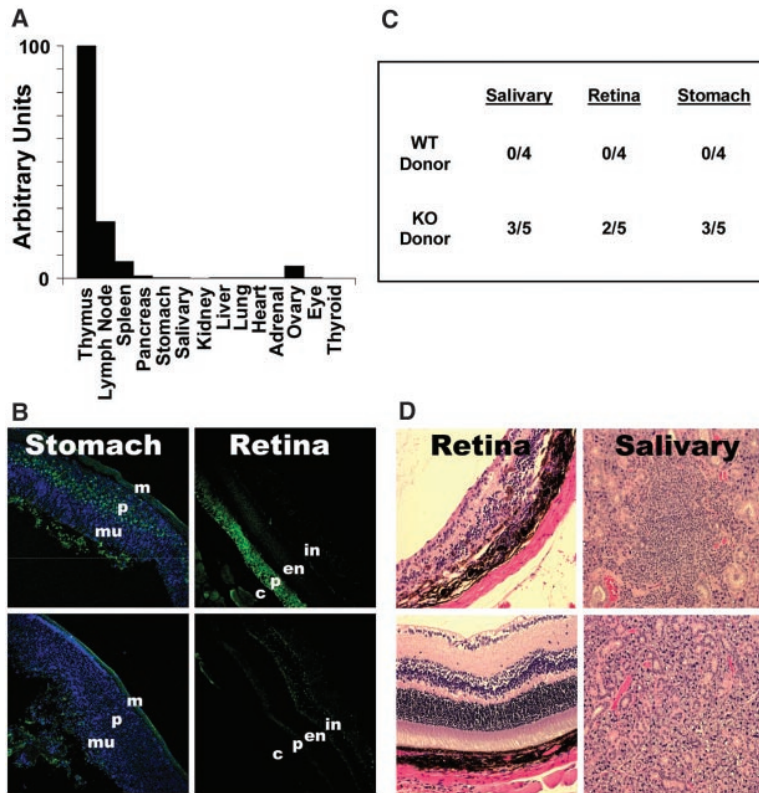


Fig. 4. The thymus is critical for aire-associated autoimmunity. (A) Aire is expressed predominantly in the thymus. Shown is relative expression of aire by quantitative real-time PCR using Taqman primers and probes on cDNA prepared from various whole organs from a 6-week-old B6 mouse. Normalization of cDNA content was done on cyclophilin; numbers represent a ratio of relative aire expression to cyclophilin expression for each tissue. For tissues other than thymus, lymph node, spleen, and ovary, aire transcripts could not be detected. Given the normalization of cDNA content by cyclophilin, the amount of aire in these tissues is at least two orders of magnitude less than the level seen in the thymus. Data shown are a representative experiment of several independent experiments. (B) Transplantation of aire-deficient thymi leads to autoantibody production. Nude mice were transplanted with either aire-deficient ($n = 3$) or wild-type thymi ($n = 6$). Six weeks after transplantation, serum was collected and tested for autoantibodies against stomach ($\times 100$) and retina ($\times 250$) by indirect immunofluorescence for recipients of aire-deficient (top panels) and wild-type control (bottom panels) thymi. Shown is representative staining from individual mice. Green indicates specific serum staining; blue (only on stomach sections) indicates staining with the nuclear marker DAPI. For the stomach, serum (3/3 knockout, 0/6 wild type) stained the parietal cell layer (p) of the stomach mucosa (mu, mucinous layer; m, muscular layer). For the retina, serum (2/2 knockout, 0/4 wild type) reacted against the outer layer containing the epithelium and rods and cones (marked p; c, choroid; en, external nuclear layer; in, inner nuclear layer). (C) Mature aire knockout lymphocytes can transfer immune infiltrates. Table summarizes immune infiltrates observed (12 weeks after transfer) in the salivary gland, retina, or stomach for Rag-deficient recipients injected with aire knockout lymphocytes or wild-type lymphocytes. Numbers represent individual mice for each group. (D) Representative immune infiltrates in tissue sections stained with H&E from Rag-deficient mice injected with lymphocytes from aire knockout mice (top panels) or wild-type control mice (bottom panels) for retina ($\times 200$) and salivary gland ($\times 100$).

autoimmune attack and indicate the importance of *aire* expression in lymphoid tissues.

To distinguish the influence of the thymus from that of peripheral lymphoid organs, and to further rule out any role for peripheral parenchymal tissues, we performed a thymus graft experiment. A thymus from either an *aire*-deficient mouse or a wild-type littermate was depleted of hematopoietic cells by incubation in 2-deoxyguanosine (31) and was then transplanted into an athymic B6^{nu/nu} recipient. Six weeks later, the generation of a peripheral T cell compartment was confirmed, and serum autoantibodies were assayed on stomach and eye sections from normal mice. Autoantibodies were found in sera from each of three mice hosting an *aire*-deficient thymus but in none of six hosts of a wild-type thymus, although the T cell compartments were reconstituted to the same level in the two cases. The pattern of autoantibody staining was the same as that seen with sera from unmanipulated *aire*-deficient mice (compare Figs. 4B and 1B). We thus concluded that *aire* must be expressed in the radioresistant stromal cells of the thymus in order to control autoimmunity in the periphery.

Influence of *aire* on T cell education.

We also established that the autoimmune disease that develops in *aire*-deficient mice is lymphocyte-autonomous. Mature lymphocytes were pooled from the spleen and lymph nodes of *aire*-deficient mice or wild-type littermates and were then transferred into alymphoid Rag^{o/o} recipients. After 12 weeks, diverse organs were assayed histologically. Lymphocytic infiltrates, similar to those observed in unmanipulated mice lacking *aire*, were found in the salivary gland, eye, and stomach of the mice that received *aire*-deficient, but not wild-type, lymphocytes (Fig. 4, C and D). These results confirm that *aire* expression in peripheral parenchymal tissues is not the factor controlling autoimmune attack.

***Aire* regulates thymic gene expression.**

Given the association between *aire* deficiency and autoimmunity, and the predominant expression of this transcription factor (25–27) in thymic MECs (4, 5), we hypothesized that *aire* controls autoimmunity by regulating the ectopic expression of peripheral tissue-restricted antigens in the medulla of the thymus. MECs were present (indeed, they were overrepresented) in *aire*-deficient mice and displayed normal levels of molecules associated with antigen presentation (fig. S5). Thus, *aire* does not dictate differentiation of MECs, nor their ability to present antigens.

To obtain a broad perspective on the transcriptional profile of MECs, we prepared RNA from cells sorted from *aire*-deficient and control littermates (sorting pooled thymocytes from five individuals as described in Fig. 2A) and used labeled complementary RNA to probe 12,000 mouse genes represented on Affymetrix

U74Av2 chips (31). Three independent experiments were performed to permit statistical treatment of the data, and three different statistical assays were applied (31). The absence of *aire* resulted in loss of or reduction in expression of a substantial number of genes (Fig. 5A), clearly more than in the randomly permuted data set. When using a factor of 5 change as an arbitrary cutoff value, decreases in transcripts of 104 genes were called significant by the Significance Analysis of Microarrays (SAM) program and 42 by the Quadrants program; decreases ranged from a factor of 5 to a factor of 70, frequently with complete extinction in mutant mice. In contrast, the number of genes induced in mutant mice did not depart from that of the random data set (14 significant by SAM, 6 by Quadrants). Thus, *aire* seems to function predominantly as a transcriptional activator. Because of statistical uncertainties linked to multiple sampling, the exact number of genes represented on the U74Av2 chip and down-regulated in the absence of *aire* cannot be ascertained, but

an estimate of 100 to 300 is a reasonable extrapolation, on the basis of the data in Figs. 5A and 6A and the statistical analysis. Similarly, it is not exactly certain what fraction of all murine transcripts are represented on the chip we used (likely 1/2 to 1/4). Therefore, the number of genes whose expression is activated by *aire* probably ranges between 200 and 1200.

If *aire* controls autoimmunity by promoting ectopic expression of peripheral antigens, one would expect a strong reduction in those genes ectopically expressed in MECs of *aire*-deficient mice. This prediction was tested (Fig. 5B) using a previously reported list of ectopic transcripts (4). Most of these genes were silenced or at least significantly repressed in MECs derived from mutant animals. This observation was solidified by closer examination of the 30 genes most strongly down-regulated in mutant MECs (Fig. 6A). Strikingly, the vast majority were ectopically expressed transcripts of peripheral tissue-restricted antigens, normally associated with functions related to the terminal differen-

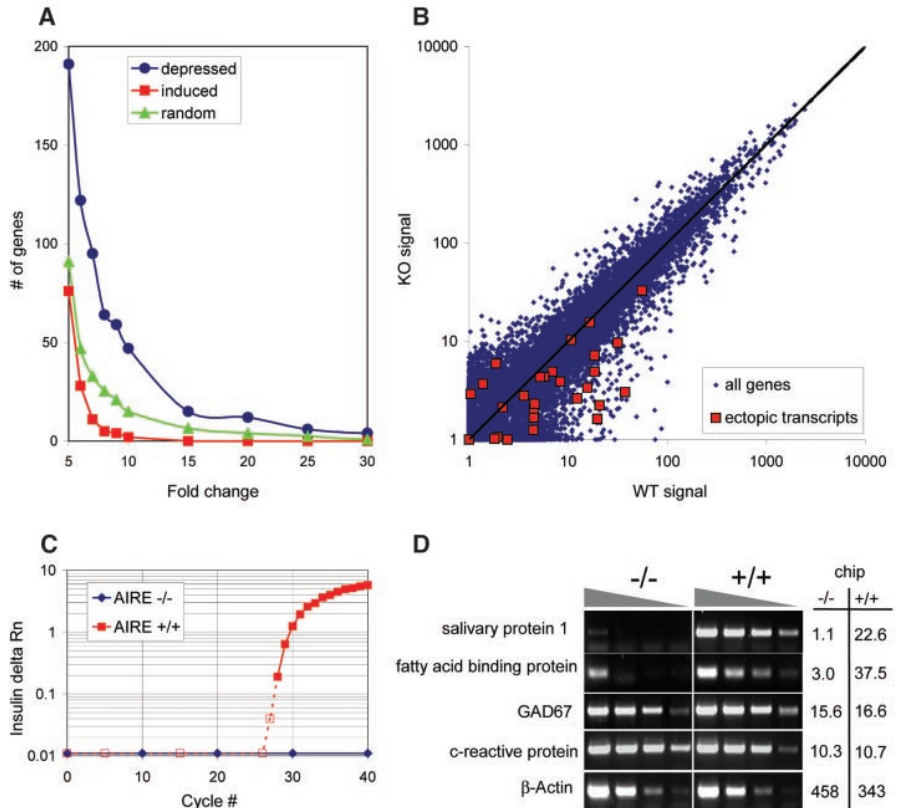
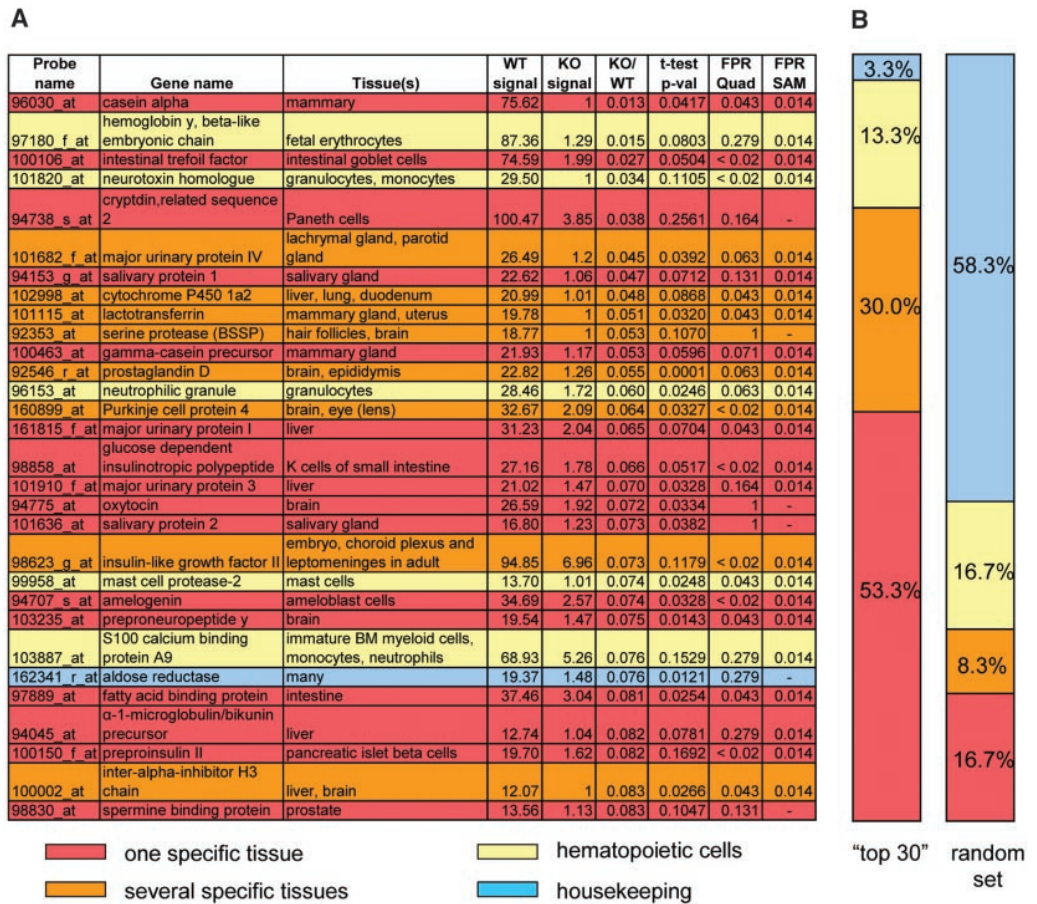


Fig. 5. Variation in gene expression in *aire*-deficient MECs. Affymetrix murine U74Av2 gene chips were hybridized with twice-amplified RNA (31) from knockout or wild-type thymic MECs. (A) The curves represent the cumulative number of genes showing the indicated relative changes in expression (fold change), either depressed (circles) or induced (squares). They are compared to a control curve derived from a randomly permuted data set (triangles). (B) Two-dimensional scatterplot of gene expression values for all genes on the chips (available at www.ncbi.nlm.nih.gov/geo, GEO series accession number GSE85), representing expression in MECs from wild-type (WT) or knockout (KO) mice. Red squares represent ectopic transcripts [described by (4)]. (C and D) Confirmation of chip expression data by real-time PCR of insulin expression (C) (normalized to cyclophilin), or by semiquantitative RT-PCR (D) (fourfold serial dilutions) of several tissue-specific genes compared with the relative expression values from the gene chips (right).

Fig. 6. AIRE primarily promotes transcription of tissue-specific genes. **(A)** The 30 genes most depressed in the aire knockout, ordered according to their expression change and color-coded according to their organismal expression patterns. These were determined with a combination of searches in the literature and of UniGene listings of expressed sequence tag distribution (NCBI). For each gene, the relative expression signal for wild-type and knockout is given, as well as the relative change in expression (KO/WT). Measures of significance included the *P* value, determined using Welch's approximate *t* test, and the false positive rate (FPR), the proportion of false positives expected at a particular level of difference between knockout and wild-type, determined using both the Quadrants (Quad) and Significance Analysis of Microarrays (SAM) programs. **(B)** The percentage of genes in (A) in each expression category compared with the percentage of genes in a random list in each category. The colors in (B) correspond to those in (A).



tiation state of cells in particular organs. Only one transcript derived from a ubiquitously expressed gene (Fig. 6A). By comparison, a random sampling of genes from the array showed that 25% fell into the category of expression in rare tissues (“one specific/several specific tissues”) and 58.3% into the ubiquitously expressed (“housekeeping”) category (Fig. 6B). Note that the genes whose expression in MECs depended on aire included a significant number expressed in tissues targeted by the autoimmune attack (e.g., salivary proteins 1 and 2, zona pellucida glycoprotein 3). In addition, we found two examples of proteins (cytochrome P450 1A2 and preproinsulin) whose expression was abolished in MECs of mutant mice and that are recognized by autoantibodies from multiple APECED patients. This observation forges a strong link between aire control of MEC transcripts and of peripheral autoimmune attack (23, 37).

To verify the relative measurements of gene expression derived from the microarray analysis, we performed quantitative real-time and semiquantitative reverse-transcription PCR (RT-PCR) analyses on cDNA from sorted MECs from aire-deficient and control littermates (Fig. 5, C and D). The results were confirmatory for the genes examined, and the find-

ings also serve to substantiate the observation that not all ectopic transcripts are dependent on aire expression. Although insulin, fatty acid-binding protein, and salivary protein-1 transcripts were absent or strongly reduced in MECs from mutant mice, genes encoding other proteins examined, such as C-reactive protein or glutamatic acid decarboxylase, were still expressed.

Discussion. These results raise several issues. First, aire seems to broadly control central tolerance induction, yet the spectrum of autoimmunity resulting from the loss of this transcription factor is quite defined. Not all peripheral organs are attacked, and within a particular organ only certain substructures are targeted. Interestingly, the defined autoimmune pattern shows many similarities to that observed in mice subjected to neonatal thymectomy (38). This pattern probably reflects a number of elements, including MHC restriction of antigens, antigen-presenting cell distributions within different organs, and blood-organ barriers. Also, ectopic transcription of different genes in thymic MECs is controlled by aire to variable degrees—some (e.g., casein- α , hemoglobin- γ) very strongly, others (trypsin 2) relatively weakly, and still others (C-reactive protein) not detectably.

One or more other transcription factor(s) might have an activity similar to aire in regulating ectopic expression of peripheral antigens in MECs, or aire may be involved in a multimeric complex that displays partial activity in its absence.

Second, the molecular mechanism by which aire controls ectopic expression of a defined battery of genes specifically in MECs is intriguing from several perspectives. It seems rather unlikely that each of these several hundred genes has an aire-binding site such as the one described in (25). More likely, aire complexes with and influences the activity of multiple other transcription factors; indeed, it is already known to interact with the common coactivator CREB-binding protein (CBP) (26). Other possibilities involve broad regulatory processes at the gene or chromatin level, such as DNA methylation, histone acetylation, nucleosome assembly, or chromatin remodeling. Any proposed mechanism will also need to account for the observation that the ectopic expression of particular peripheral genes was restricted to a small subset of MECs (5). This latter point may underlie our observation that the specific substructures targeted for a particular organ can differ in different individuals—for the eye, autoantibodies directed at the rod and cone layer of the retina in

one mouse (Fig. 1D), to other retinal layers in another mouse (32).

Finally, it is worth considering aire-deficient mice as a model of APECED. Like human patients, the murine model shows multiorgan attack by lymphocytic infiltrates and recognition by serum autoantibodies. In both cases, there is disease heterogeneity between individuals and exacerbation with age. The differences between humans and mice in the spectrum of organs targeted could well be due to the influence of genetic modifiers, as recently described for the HLA locus in humans (39). Aire-deficient mice should prove invaluable for dissecting the relative importance of genetic, environmental, and stochastic processes in determining the target organ specificity of autoimmune destruction.

References and Notes

1. K. M. Garza, V. S. Chan, P. S. Ohashi, *Rev. Immunogenet.* **2**, 2 (2000).
2. D. Hanahan, *Curr. Opin. Immunol.* **10**, 656 (1998).
3. L. Klein, B. Kyewski, *Curr. Opin. Immunol.* **12**, 179 (2000).
4. J. Derbinski, A. Schulte, B. Kyewski, L. Klein, *Nature Immunol.* **2**, 1032 (2001).
5. L. Klein, B. Roettinger, B. Kyewski, *Eur. J. Immunol.* **31**, 2476 (2001).
6. P. Naquet, M. Naspetti, R. Boyd, *Semin. Immunol.* **11**, 47 (1999).
7. H. Kishimoto, J. Sprent, *Clin. Immunol.* **95**, S3 (2000).
8. C. Jolicoeur, D. Hanahan, K. M. Smith, *Proc. Natl. Acad. Sci. U.S.A.* **91**, 6707 (1994).
9. K. M. Smith, D. C. Olson, R. Hirose, D. Hanahan, *Int. Immunol.* **9**, 1355 (1997).
10. M. W. Hoffmann, J. Allison, J. F. Miller, *Proc. Natl. Acad. Sci. U.S.A.* **89**, 2526 (1992).
11. M. W. Hoffmann, W. R. Heath, D. Ruschmeyer, J. F. A. P. Miller, *Proc. Natl. Acad. Sci. U.S.A.* **92**, 9851 (1995).
12. M. G. Von Herrath, J. Dockter, M. B. A. Oldstone, *Immunity* **1**, 231 (1994).
13. A. M. Sponaas et al., *Int. Immunol.* **6**, 277 (1994).
14. S. J. Antonia, T. Geiger, J. Miller, R. A. Flavell, *Int. Immunol.* **7**, 715 (1995).
15. M. Oukka, M. Cohen-Tannoudji, Y. Tanaka, C. Babinet, K. Kosmatopoulos, *J. Immunol.* **156**, 968 (1996).
16. L. Klein, T. Klein, U. Ruther, B. Kyewski, *J. Exp. Med.* **188**, 5 (1998).
17. M. Oukka et al., *Immunity* **4**, 545 (1996).
18. L. Klein, M. Klugmann, K.-A. Nave, V. K. Tuohy, B. Kyewski, *Nature Med.* **6**, 56 (2000).
19. A. C. Anderson et al., *J. Exp. Med.* **5**, 761 (2000).
20. A. Pugliese et al., *Nature Genet.* **15**, 293 (1997).
21. P. Vafiadis et al., *Nature Genet.* **15**, 289 (1997).
22. C. E. Egwuagu, P. Charukamnoetkanok, I. Gery, *J. Immunol.* **159**, 3109 (1997).
23. P. Björnses, J. Aaltonen, N. Horelli-Kuitunen, M. L. Yaspo, L. Peltonen, *Hum. Mol. Genet.* **7**, 1547 (1998).
24. P. Peterson et al., *Immunol. Today* **19**, 384 (1998).
25. P. G. Kumar et al., *J. Biol. Chem.* **276**, 41357 (2001).
26. J. Pitkanen et al., *J. Biol. Chem.* **275**, 16802 (2000).
27. P. Björnses et al., *Am. J. Hum. Genet.* **66**, 378 (2000).
28. M. C. Rosatelli et al., *Hum. Genet.* **103**, 428 (1998).
29. S. Zuklys et al., *J. Immunol.* **165**, 1976 (2000).
30. C. Ramsey et al., *Hum. Mol. Genet.* **11**, 397 (2002).
31. See supporting data on Science Online.
32. M. S. Anderson et al., data not shown.
33. K. Nagamine et al., *Nature Genet.* **17**, 399 (1997).
34. M. Halonen et al., *J. Histochem. Cytochem.* **49**, 197 (2001).
35. M. Heino et al., *Biochem. Biophys. Res. Commun.* **257**, 821 (1999).
36. M. Heino et al., *Eur. J. Immunol.* **30**, 1884 (2000).
37. M. Gylling et al., *J. Clin. Endocrinol. Metab.* **85**, 4434 (2000).
38. A. Kojima, R. T. Prehn, *Immunogenetics* **14**, 15 (1981).
39. M. Halonen et al., *J. Clin. Endocrinol. Metab.* **87**, 2568 (2002).

40. We thank G. Losyev, Q.-M. Pham, J. Rasmussen, and R. Saccone for help with flow cytometry, mice, microarray software and chip analysis, respectively, and E. Smith for assistance with the figures. Supported by the W. T. Young Chair fund, NIH grant RO1 DK60027-01 (D.M. and C.B.), Joslin Diabetes Center grant DERC 2 P30 DK36836-16, a Howard Hughes Medical Institute Postdoctoral Fellowship for Physicians and NIH grant KO8-DK59958-01A1 (M.S.A.), an NSF Graduate Research Fellowship and NIH training grant 2T32 DK07260-26 to Joslin Diabetes Center (E.S.V.), Irvington Institute for Immunological Research (L.K.), Juvenile Diabetes Research Foundation (Z.C.), Human Frontier Science Program (S.B.), and an NRSA fellowship in Cancer Immunology (T32CA70083-05) and the Cancer Research Institute (S.J.T.).

Supporting Online Material

www.sciencemag.org/cgi/content/full/1075958/DC1
Materials and Methods
Figs. S1 to S8
References

10 July 2002; accepted 19 September 2002
Published online 10 October 2002;
10.1126/science.1075958
Include this information when citing this paper.

REPORTS

Broadband Modulation of Light by Using an Electro-Optic Polymer

Mark Lee,* Howard E. Katz, Christoph Erben, Douglas M. Gill, Padma Gopalan, Joerg D. Heber, David J. McGee

A major challenge to increasing bandwidth in optical telecommunications is to encode electronic signals onto a lightwave carrier by modulating the light up to very fast rates. Polymer electro-optic materials have the necessary properties to function in photonic devices beyond the 40-GHz bandwidth currently available. An appropriate choice of polymers is shown to effectively eliminate the factors contributing to an optical modulator's decay in the high-frequency response. The resulting device modulates light with a bandwidth of 150 to 200 GHz and produces detectable modulation signal at 1.6 THz. These rates are faster than anticipated bandwidth requirements for the foreseeable future.

Transmitting signals by using infrared light through optical fiber is the most effective way to move large amounts of data rapidly over long distances. Consequently, optical communications form the backbone of the Internet and telephone networks, and they are envisioned to carry real-time multimedia content in the future.

Bell Laboratories—Lucent Technologies, 600 Mountain Avenue, Murray Hill, NJ 07974, USA.

*To whom correspondence should be addressed, E-mail: markl@lucent.com

Approaches to increasing optical bandwidth are being pursued to accommodate anticipated growth in data traffic. At present, high-speed optical networks use bandwidths of 10 GHz (~10 billion bits per second) per channel, and 40-GHz products are being introduced. Basic research efforts are aiming to push bandwidths to 80, 100, and even 160 GHz.

Expanding bandwidth beyond 100 GHz involves many scientific and engineering challenges, among which is the encoding of electronic data signals onto a lightwave carrier by

modulating the light in phase or amplitude. This is usually done with an electro-optic (E-O) modulator (*I*), where a signal voltage changes the refractive index of an E-O dielectric optical waveguide, modulating the phase of a guided lightwave. Amplitude modulation is obtained by generating a phase difference $\Delta\Phi$ between light in two coherent waveguides and then combining to produce constructive or destructive interference. In present technology, lithium niobate is the E-O material most widely used in high-speed optical modulators.

An E-O device produces the strongest modulation when $\Delta\Phi = \pi$ radians. For an input voltage V_{in} , $\Delta\Phi \propto \pi(V_{in}/V_{\pi})$, where V_{π} is the "half-wave" voltage that makes $\Delta\Phi = \pi$ near zero frequency [direct current (dc)], is:

$$V_{\pi} = \frac{\lambda_0 d}{2n_{opt}^3 \Gamma L} \quad (1)$$

where λ_0 is the carrier wavelength, d is the gap between voltage electrodes, n_{opt} is the optical refraction index, r is the E-O coefficient of the dielectric, L is the device length, and Γ is defined as the signal electric field in the optical waveguide normalized to the field that would be there if air were the dielectric. The central problem for high-speed operation is that, for a fixed V_{in} , $\Delta\Phi$ decreases as modulation frequency increases. This response deterioration has three physical origins. The first is dissipation of V_{in} due to resistance in the electrodes guid-

Supplementary Material

Materials and Methods

1. Targeting vector and knockout mice

The murine *aire* gene was cloned from a bacteriophage mouse Sv/129 genomic library using a PCR product off of mouse genomic DNA corresponding to a region from exons 1 and 2 as a probe. A single *lox* site was introduced between exons 1 and 2 by the use of oligonucleotide linkers at a XcmI site. A cassette containing the P_{gk}-neo flanked by *lox* recombination sites was introduced at a XbaI site between exons 3 and 4. The orientation of the *lox* sites and their flanking regions was confirmed by DNA sequencing. A linearized 7.5 kb fragment was prepared by digestion with NdeI (Fig. S1) and was used to electroporate the D3 cell line as previously described (1). ES clones were initially screened as described in Fig. S1. An additional confirmatory Southern blot was performed by digesting genomic DNA with SspI and probing with a PCR product from genomic DNA downstream of the 3' NdeI site (an external probe). Wild type DNA will give a 7.8 kb fragment while the recombined allele will give a 9.8 kb fragment and this was confirmed on two independent clones. Clones carrying the homologous recombination event were injected into C57Bl/6 blastocysts. Chimeras were bred onto C57Bl/6 and offspring with germline transmission of the altered *aire* allele were subsequently bred to CMV-Cre transgenic mice on the C57Bl/6 background (2) for *in vivo* deletion of the second exon as shown in Fig. S1. For genotyping of mice two PCR reactions were performed with the following primers: Set 1- GTCATGTTGACGGATCCAGGGTAGAAAGT and AGACTAGGTGTTCCCTCCCAACCTCAG. Wild type mice give a product of 1150 bp,

while knockout mice give a product of 690 bp. Set 2-
ATAGCACCCACGACACCCAAG and ATATCATTCTCCAACCTGCCTCTTT.
Wild type mice give a product of 507 bp, while knockout mice do not give any product.
Homozygous aire-deficient mice were first generated by intercrossing of heterozygous
animals. Mice used for experiments here were generated by intercrossing heterozygous
mice after Cre-deletion and were of the F2xF2, F2xF3, or F3xF3 generation of a
backcross to C57Bl/6. Aire-deficient mice appeared healthy, and were normally active
and mobile. Young homozygous males and females were fertile, while breeding
performance from homozygous males and females seemed less optimal after 3 to 4
months of age. All mice were maintained under barrier conditions at the Harvard
Medical School animal facility; IACUC approval # 02954.

2. Histology

Organs from mice were harvested and fixed overnight in 10% formalin, embedded in
paraffin, sectioned, and stained for H&E at the Rodent Core Histology Laboratory at
Harvard Medical School. Immune infiltrates of organs were confirmed and scored by
independent reading of the slides with a mouse pathologist.

3. Immunological analyses

a. Lymphoid populations

Cell suspensions were teased from the major lymphoid organs and analyzed by
multiparameter flow cytometry after immunostaining with cocktails of fluorescent
antibodies. For thymic T cells, the reagents used included anti-CD3, anti-CD5, anti-
CD24, anti-CD25, anti-CD69, anti-CD44, anti- $\alpha\beta$ -TCR, anti-DX5 anti-CD45R(B220),
anti-DX5 conjugated with either FITC, phycoerythrin or biotin (all Pharmingen), anti-

CD4-FITC and anti-CD8-FITC (Caltag), anti-peanut agglutinin(PNA)-FITC (Sigma), anti-CD4-PE-Texas Red, anti-CD8-PE-Texas Red (Caltag), anti-CD4-Cychrome, anti-CD8-Tricolor (Caltag). Biotinylated reagents were detected using streptavidin-FITC (Pharmlingen) or streptavidin-PE-Texas Red (Caltag). For analyses of bone marrow, spleen and lymph nodes, antibodies used include anti-IgD-FITC (clone 11-26c.2a, BD Pharmlingen), anti-CD69-FITC (H1.2F3, BD Pharmlingen), anti-CD62L-FITC (Mel14, BD Pharmlingen), anti-TCR β -FITC or -Cychrome (H57-597, BD Pharmlingen), anti-IgM-PE (R6-60.2, BD Pharmlingen), anti-CD44-PE (IM7, BD Pharmlingen), anti-CD8a-Tri-color (5H10, Caltag), anti-CD19-Tri-color (6D5, Caltag), anti-CD4-PE-Texas Red (RM4-5, Caltag) and anti-CD45R (B220)-PE-Texas Red (RA3-6B2, Caltag).

b. Dendritic cells

Thymus, spleen and lymph node (subcutaneous and mesenteric lymph nodes analyzed independently) suspensions were prepared according to a previously described method (3) that ensures release of DCs from tissues. Briefly, organs were digested in Ca²⁺-free buffer containing collagenase D (Roche Molecular Biochemicals) at 37°C for 20 minutes. Digests were vigorously pipetted and filtered over nylon mesh in buffer containing 5mM EDTA. Cells were washed and spleen suspensions were subjected to RBC lysis. For 6-color flow cytometric analysis, cell suspensions were stained for 30 minutes at 4°C in PBS/2% FCS with the following monoclonal antibodies: FITC-I-A^b, PE-CD11c, CD4-PE/TR, B220-PE/Cy7 (Pharmlingen), and CD8 α -APC (FITC-I-A^b and PE-CD11c were purchased from Pharmlingen; all other mAbs from Caltag). Cell suspensions were analyzed immediately after staining to avoid fixation artifacts. Hoescht 33342 (Calbiochem) was added to all samples shortly before analysis for dead cell exclusion.

c. Thymic epithelial cells

Thymic epithelial cells (TEC) were prepared largely according to (4). Briefly, 5 thymi of young adult (3-5 weeks old) animals were digested for 30-40 minutes with collagenase / dispase (0.2mg/ml each) in RPMI + 2% FCS in the presence of 25µg/ml DNase. EDTA was added to a final concentration of 10 mM for the last 5 minutes. Cells were then separated on a discontinuous Percoll density gradient. The TEC-enriched fraction was harvested and stained with purified CDR1, followed by F(ab')₂ anti-rat phycoerythrin (PE) (Southern, Birmingham, Alabama). After incubation in 4% rat-serum for ten minutes, cells were then stained with biotinylated anti-B7 (Pharmingen) or anti MHC class II (P7/7), followed by streptavidin PE-Texas Red, G8.8-FITC and anti CD45 allophycocyanin (Southern). Medullary epithelial cells were sorted according to the phenotype CD45⁻, G8.8⁺, CDR1^{int} and B7.1⁺.

d. Autoantibodies

Sera were prepared from tail vein bleeds (100 µl). Autoantibodies for stomach, salivary, pancreas, liver, retina, and ovary were detected by indirect immunofluorescence and thyroid autoantibodies were detected by ELISA as described below. ELISA assays for anti-thyroglobulin Ab's were performed on plates coated overnight with bovine thyroglobulin (Sigma) at 1 µg/ml. Plates were subsequently washed and then incubated with serum starting at a 1:50 dilution with serial two-fold dilutions. Ab's were then detected with an alkaline phosphatase conjugated rat anti-mouse IgG (Jackson Immunoresearch). Serum from several 12 week old MRL.lpr/lpr mice were used as a positive control as these mice have previously been shown to harbor anti-thyroglobulin antibodies (5). For immunofluorescence, 7 µm cryostat sections were prepared from a

number of organs of adult RAG-deficient mice (The Jackson Laboratory), to avoid interference from endogenous immunoglobulins, and stained largely as described (6), with 1/40 dilutions of sera from knockout mice or control littermates, counterstained with FITC-conjugated goat anti-mouse IgG (Jackson ImmunoResearch). Again, serum from MRL.lpr/lpr was used as a positive control. In some experiments, DAPI (Molecular Probes; 5 min @ 300 nM) was included in the last wash for identification of nuclei. Slides were examined on a Zeiss Axiophot2 microscope, with 5x, 10x and 20x lenses. Reading of the presence of positive staining was done in a blinded fashion. Photographs were taken on a Zeiss LSM 410 confocal microscope.

e. T cell responses

Antigen presentation assays were performed by purifying splenic cells from mice and plating them out at 5×10^5 cells/well with T cell hybridomas at 5×10^4 cells/well and antigen in a 96 well plate. 24 hours later supernatants were collected and incubated with washed CTLL indicator cells for measurement of IL-2 production. CTLL plates were pulsed with ^3H -Thymidine during the last 6 hours of a 24 hour culture. Mixed lymphocyte reactions were performed by purifying splenic cells as stimulators and inguinal lymph node cells as responders. Cells were mixed at 4×10^5 cells/well in a 96 well plate at a 1:1 and a 1:2 ratio of responders:stimulators. Controls of responders alone, stimulators alone, responders with self stimulators, and a positive control with ConA were performed in parallel. Cultures were pulsed with ^3H -Thymidine on day 4 to 5 of culture. For anti-CD3/CD28 stimulation, naïve lymph node cells were purified from 4 week old mice and cultured in plates coated with anti-CD3 and anti-CD28 (Pharmingen) at $10\mu\text{g/ml}$ each at 37°C for 4 hours at 1×10^6 cells/well in 24 well plates. Supernatants

were harvested on day 1 and 2 of culture and assayed for IL-2, IL-4, and γ -IFN by a sandwich ELISA with standards (Pharmingen).

f. Bone marrow chimeras

Bone marrow chimeras were generated by lethal irradiation of 4 to 5 week old mice (1000 rads). Bone marrow was harvested from 4 to 5 week old knockout or wild type mice and mature T cells were depleted by using anti-CD4 and anti-CD8 antibodies (Pharmigen) and magnetic bead depletion of antibody conjugated cells (Dynabeads). Greater than 90% depletion of CD4 and CD8 cells was confirmed by flow cytometry. 10×10^6 bone marrow cells were then injected into the tail vein of the irradiated recipients. The chimeras were analyzed two months after reconstitution for tissue infiltrates by histology and autoantibody detection.

g. Thymic transplants

Thymi were isolated from newborn knockout or wild type mice and cultured in 1.35 mM 2-deoxyguanosine (Sigma) for six to eight days to deplete bone marrow derived cells. The thymi were then washed in media for 2 hours and transplanted under the kidney capsule of adult nude mice (6 to 8 weeks of age) on the C57Bl/6 background (The Jackson Laboratory). 6 weeks after transplantation whole blood and serum was collected. T cell reconstitution of all transplanted mice was confirmed by FACS analysis of whole blood for CD4, CD8, CD3, and B220. Serum was used for autoantibody detection by indirect immunofluorescence as previously described.

h. Mature lymphocyte transfers

Lymphocytes were prepared by mechanically disrupting the spleen and lymph nodes collected from 9 to 10 week old knockout or wild type mice. A 1:1 mixture of splenic to

lymph node cells from individual mice was resuspended in PBS and 40×10^6 cells were injected into the tail vein of sublethally irradiated (350 rads) adult Rag^{0/0} mice on the C57Bl/6 background (The Jackson Laboratory). Mice were sacrificed 12 weeks after the transfer and analyzed for tissue infiltrates by histology.

4. Gene expression analyses

a. RNA preparation

Total RNA from whole organs was prepared as previously described (7). For sorted mTEC's, total RNA was prepared using the High Pure RNA Isolation Kit (Roche). The standard kit protocol for isolation of total RNA from cultured cells using guanidine hydrochloride was followed. RNA was eluted in sterile, RNase –free water. It was quantitated by real-time PCR using a GAPDH-specific probe, in comparison with a spleen RNA standard of known concentration.

b. Semi-quantitative PCR

Semi-quantitative PCR analyses were performed using a 4-fold dilution series of input cDNA. Primer pairs used for the detection of specific gene products were designed to span at least one intron. The following oligonucleotide pairs were used: β -actin: TGGAATCCTGTGGCATCCATGAAAC and TAAAACGCAGCTCAGTAACAGTCCG; Insulin: AGACCATCAGCAAGCAGGTC and CTGGTGCAGCACTGATCCAC; iFabp: AGACGGAACGGAGCTCAC and GCTCTTCAGCGTTGCTCC; GAD67: TGCAACCTCCTCGAACGCGG and CCAGGATCTGCTCCAGAGAC; C-reactive protein: CCATGGAGAAGCTACTCTG and CCCAAGATGATGCTTGC; Salivary protein 1: GGCTCTGAAACTCAGGCAGA and TGCAAACCTCATCCACGTTGT. PCR reactions were carried out in a final volume

of 30µl, using 1.5 U of REDTaq DNA Polymerase (Sigma) and 250 nM of each primer in 1 x PCR-buffer (Sigma). Cycling conditions were a single denaturing step at 94°C for 3 min followed by either 35-40 cycles (for tissue-specific genes) or 25 cycles (for actin normalization) of 94° C for 45 seconds, 50°-54° C for 45 seconds and 72° C for 1 min, followed by a final extension step of 72° C for 3 min.

c. Real-time PCR

Real-time PCR was carried out on cDNA prepared from Dnase-treated RNA. For *aire*, the following primers were used: Forward-CCAGTGAGCCCCAGGTTAAC
Reverse-GACAGCCGTCACAACAGATGA Probe-FAM-TCACCTCCGTCGTGGCACACG-TAMRA. For insulin, the following primers were used: Forward-CTTCAGACCTTGGCGTTGGA Reverse-ATGCTGGTGCAGCACTGATC Probe-FAM-CCCGGCAGAAGCGTGGCATT-TAMRA. For normalization, primers for cyclophilin were used: Forward-CAGACGCCACTGTGCTTT Reverse-TGTCTTTGGAACCTTTGTCTGCAA Probe-VIC-CCCTTGGGCCGCGTCTCCTT-TAMRA. Real-time PCR reactions were carried out in a final volume of 25µl with 900nM of the forward and reverse primers and 200nM of the probe using 2X Taqman Master Mix (Applied Biosystems) containing AmpliTaq Gold polymerase. Reactions were run on an Applied Biosystems 7700 Sequence Detection System machine in duplicate. For analysis of *aire* gene expression from organ-derived cDNA, the standard curve method was used as previously described (REF Heid et al). The standard curves for both *aire* and cyclophilin had R² values >0.95.

d. Microarrays: probe preparation and hybridization

In order to have enough RNA for Affymetrix gene chip hybridization, total mTEC RNA was amplified using a T7 polymerase-based method. Using the MessageAmp aRNA Kit (Ambion), total RNA (typically 50-100 ng) was reverse transcribed using an oligo(dT)-T7 promoter primer to prime the first strand synthesis. After second strand cDNA synthesis, the double-stranded cDNA was purified using the MessageAmp filter cartridges and solutions as directed. The purified cDNA product was concentrated in a heated vacuum centrifuge (Eppendorf Vacufuge set at 30° or 45°), then transcribed using T7 RNA polymerase as per the MessageAmp protocol. The resulting amplified antisense RNA (aRNA) was purified using the MessageAmp filter cartridges and reagents, then quantitated using a spectrophotometer (Beckman DU530). The aRNA yield from the first round of amplification was usually 5-15 µg, and the 260:280 absorbance ratios were normally between 1.8 and 2.1. Two µg of the first-round aRNA (concentrated by vacuum centrifugation, if necessary) was used for the second round of amplification. This aRNA was again reverse transcribed, with first strand synthesis primed with a random hexamer primer, and second strand synthesis primed with an oligo(dT)-T7 promoter primer, as directed by the MessageAmp protocol. Again using the MessageAmp filter cartridges and reagents, the resulting double-stranded cDNA was purified, then concentrated to less than 44 µL. Half of the concentrated cDNA was next used in a second round of in vitro transcription, performed using the BioArray High Yield RNA Transcript Labeling Kit (Enzo Diagnostics) as directed, with a 5-hour incubation at 37°. In this second round of transcription, biotinylated ribonucleotides were incorporated into the aRNA as it was transcribed by T7 RNA polymerase. The labeled aRNA was purified using the RNeasy Mini Kit (Qiagen), then quantitated using a spectrophotometer. Typical labeled aRNA

yields ranged from 45-90 µg, and the 260:280 absorbance ratio was between 2.0 and 2.3. Final aRNA concentration was no less than 0.6 µg/µl. 5X fragmentation buffer (200mM Tris-acetate, pH 8.1, 500 mM KOAc, 150 mM MgOAc) was added to 15 µg of the biotinylated aRNA, and this mixture was heated at 94° for 35 minutes. After fragmentation, the aRNA was hybridized to a Test3 Array (Affymetrix), an all-purpose control gene chip representing housekeeping genes. This was done to determine the quality of the probe, reflected by the 3':5' ratio of the aRNA probes before hybridization to the actual U74Av2 gene chips. The 3':5' ratios of the amplified aRNA probes were normally between 4 and 15. The Test3 Arrays and the U74Av2 arrays were both hybridized for 16 hours at 45° with constant rotation at 60 rpm. Next, they were washed and conjugated with streptavidin-phycoerythrin in the Fluidics Station 400 (Affymetrix). Finally, each chip's fluorescence was read on a GeneArray Scanner (Affymetrix), an Argon laser detector.

e. Microarray data processing

The initial fluorescence reads from the Affymetrix fluorescence detector were first processed to determine raw expression values using Affymetrix MicroArray Suite 5.0. These raw reads from three independent experiments were normalized using the Norm software (8). Briefly, this S-Plus application normalizes expression values in comparable datasets, not simply standardized relative to the mean of each dataset (which introduces severe distortions), but relative to a spline fitted curve encompassing the full range of raw data points. This spline normalization curve is calculated as a locally smoothed regression from a set of 125 reference points (genes chosen as the 1% most rank-invariant between all datasets, and covering the whole range of expression values). Raw and

“normed” expression values for each dataset are available at www.ncbi.nlm.nih.gov/geo; accession numbers X-XXXXXXX.

The “normed” values were then processed with two software packages, “Significance Analysis of Microarrays” (SAM) (8) and “Distill” (8). For SAM processing, the input data was not in logarithmic form, 100 permutations were used, the fold change value was set at 5, and the delta value was set at 0.5. The “Distill” package 1) calculates average gene expression values from parallel datasets, after outlier elimination (outlier detection based on a jackknife algorithm, in which “noisy” datapoints are rejected if they lead to a greater than z -fold increase in the gene-wise variance; z set at 20 in these analyses); 2) estimates with Welch’s t-test the gene-wise p-value of significance between datasets from variant (V, here homozygous knockout) and reference (R, here wild type littermate) conditions; these p-values are to be considered as indicative only, as the estimate of gene-wise variance on small datasets is very unreliable, and the p-values are not corrected for multiple sampling (see (9)). 3) calculates the false-positive-ratio (FPR $-(10)$), a parameter far more applicable than gene-wise p-values in experimental settings where the number of replicates between identical conditions is experimentally realistic yet statistically low. The algorithm analyzes the reproducibility of expression ratios (“Fold Change”, FC) between the variant and reference conditions in N independent experiments ($FC_{1 \rightarrow N}$), essentially deriving significance from the distribution of FC values in the repeated experiments: expression ratios that deviate from 1 because of true variation will be reproduced in successive experiments, while those due to biological or experimental noise will show unrelated FC. For incremental values of FC (x ranging from 2 to the maximum observed FC), the program calculates the frequency of reproducible

observations ($FC_{1 \rightarrow N}$ all $>x$ or $<1/x$), and the frequency of noise observations in the dataset (combination of $FC_{1 \rightarrow N} >x$ and $<1/x$). These frequencies are then compared to those of “pseudo-reproducible” observations in a simulated control dataset of identical dimension, generated by random reassortment of the data (resampling within gene and experiment). As can be expected, the FPR calculated in this manner is very high at low fold-change values, even with datasets of good quality, but quickly drops off for FC greater than 5. This approach thus carries a significant penalty in terms of false-negative calls, in that a single $FC_{i,N}$ mis-determination eliminates the corresponding gene (unavoidable for $2 < N < 4$).

Supplementary Text

Additional data

1. Analysis of lymphoid organs

a. Thymus

T cell differentiation in the thymus of aire-deficient (aire^{0/0} or KO) mice was compared to that of wild type (WT) mice using a panel of maturity-related cell surface antigens. The differential expression of CD4 and CD8 (Fig. S2, left panels) indicated that all major thymocyte subsets were present in the KO thymus in similar proportions to WT mice.

More sophisticated analysis was used to assess other compartments, including the most immature CD3⁻CD4⁻CD8⁻B220⁻CD11b⁻ cells (DN; Fig. S2 far right panels), further distinguished by CD44 and CD25 staining; post-positive selection cells identified by CD69 positivity (Fig. S2 middle right panel); in the aire-deficient mice as in control littermates, transitional intermediates as well as more mature cells are visible on the $\alpha\beta$ -TCR^{hi} plot (Fig. S2 middle left panel). For these, and all other subsets tested (11), no significant differences were observed between KO and WT mice with regard to the size and proportion of thymocyte subsets.

b. Bone marrow

B cell differentiation in the bone marrow of aire^{0/0} mice was compared to that of WT mice by flow cytometry. Total cell counts were comparable. B cell maturation was assessed by flow cytometric analysis of CD19, IgM and IgD expression. The percentage of CD19⁺ cells in the bone marrow of aire^{0/0} mice was normal. As shown by the

IgM/B220 plot in Fig. S2A, the early progression through pro- and pre-B stages is comparable in both types of mice. B-cell maturation in bone marrow through IgM⁺IgD⁻, IgM⁺IgD⁻, IgM^{hi}IgD^{hi} and IgM^{lo}IgD^{hi} stages was also unaffected by the deficiency (11).

c. Spleen and lymph nodes

Spleens and lymph nodes from WT and KO mice were also analyzed by H+E or immunofluorescence staining with antibodies against CD4, CD8, TCR β and IgM. Gross morphology of spleens and lymph nodes in *aire*^{0/0} mice was not altered. T-cell zones and B-cell follicles were properly formed in deficient animals (11).

Mature B- and T-cell subsets in spleen and lymph nodes were analyzed by flow cytometry in *aire*^{0/0} mice and control littermates (Fig. S2B and C). Although total cell number in spleens was comparable in both types of mice, lymph nodes in KO mice appeared to have modestly higher numbers of cells than that in WT controls ($2.5 \pm 1.2 \times 10^6$ vs. $5.6 \pm 2.6 \times 10^6$ for cervical LNs and $1.3 \pm 0.8 \times 10^6$ vs. $2.1 \pm 0.8 \times 10^6$ for inguinal LNs in WT and KO mice, respectively; n=5), perhaps reflecting the increased cell activation driven by autoreactivity. The relative abundance of T and B cells was normal in the mutant mice (Fig. S2B, left panel). B cell distribution in subpopulations also appeared normal, as illustrated by the IgD/IgM stain (Fig. S2B, middle panel). Finally, reflecting the normal population distribution in the thymus, CD4/CD8 ratios were preserved in the periphery (Fig. S2B, right panel).

To analyze regulatory T cells, gated CD4⁺ splenocytes were analyzed for expression of CD25 and CD69. The former should reveal “regulatory” populations of CD4⁺CD25⁺ cells with the CD69 marker aiding in the distinction of naïve from activated

cells. As illustrated in Fig. S2C, no difference was observed in the frequency of CD4⁺CD25⁺ cells in aire-deficient mice compared to control littermates.

Naïve T cell responses were also analyzed by harvesting bulk splenocytes or lymph node cells and stimulating them in culture with immobilized anti-CD3 and anti-CD28. Supernatants were collected at 24 and 48 hours post-stimulation and levels of IL-2, IL-4, and γ -IFN were measured. As shown in Figure S3, no difference in cytokine production was seen between WT and KO mice.

d. Dendritic cells and antigen presentation

To test for alterations in dendritic cells (DCs) due to aire deficiency, we analyzed DC populations in thymus, spleen, and lymph nodes (gut and subcutaneous) from WT and KO mice at different ages. Multiple subcutaneous lymph nodes (cervical, axillary, brachial, and inguinal lymph nodes) were pooled for analysis in most experiments although cervical lymph nodes were also analyzed separately. Myeloid and lymphoid DC subsets were analyzed by staining for CD8 α and CD4 in combination with classical DC markers (CD11c and MHC class II). The myeloid and lymphoid DC subsets were phenotypically similar between WT and KO tissues. The abundances of different DC subsets were also comparable, although an expansion in the CD4⁺ DC subset was observed in several KO mice at 3 and 4 weeks of age. For the most part, levels of MHC class II on all subsets appeared similar between WT and KO animals. MHC class II levels were occasionally elevated in gut and subcutaneous lymph node DCs from 9 and 15 week old aire-deficient mice.

To analyze function of antigen presenting cells (APC's), splenocytes were harvested from WT or KO mice and cultured with antigen specific T cell hybridomas at limiting concentrations of antigen or peptide. Illustrated in Fig. S5 is an example of such an assay for presentation of hen egg lysozyme (HEL) or HEL-peptide showing that WT and KO APC's present at similar levels to T cell hybridomas. Similar results were seen with a second T cell hybridoma specific for ovalbumin (11).

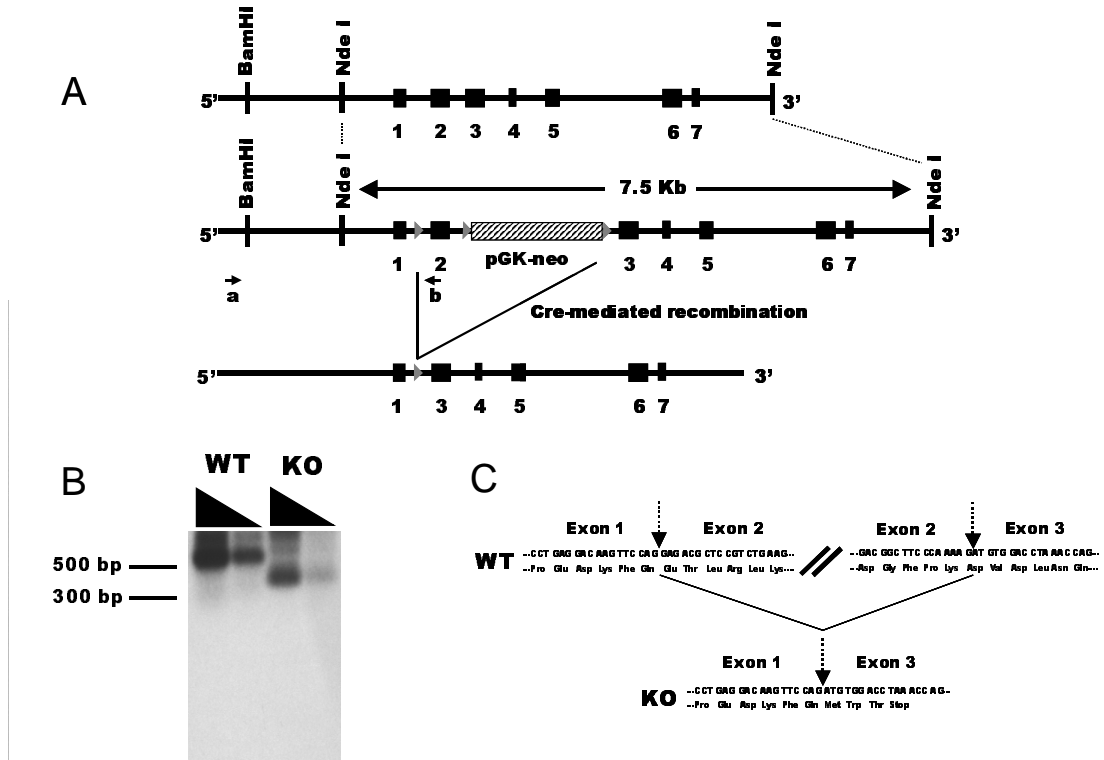
2. Immunological tolerance

To measure *in vitro* tolerance to self, mixed lymphocyte reactions (MLR's) were carried out with WT or KO derived splenocytes (stimulators) and lymph node cells (responders). Shown in Fig. S7 is a representative experiment showing that KO responder cells do not have any increased proliferation to self-APC's over WT or C57Bl/6 responders.

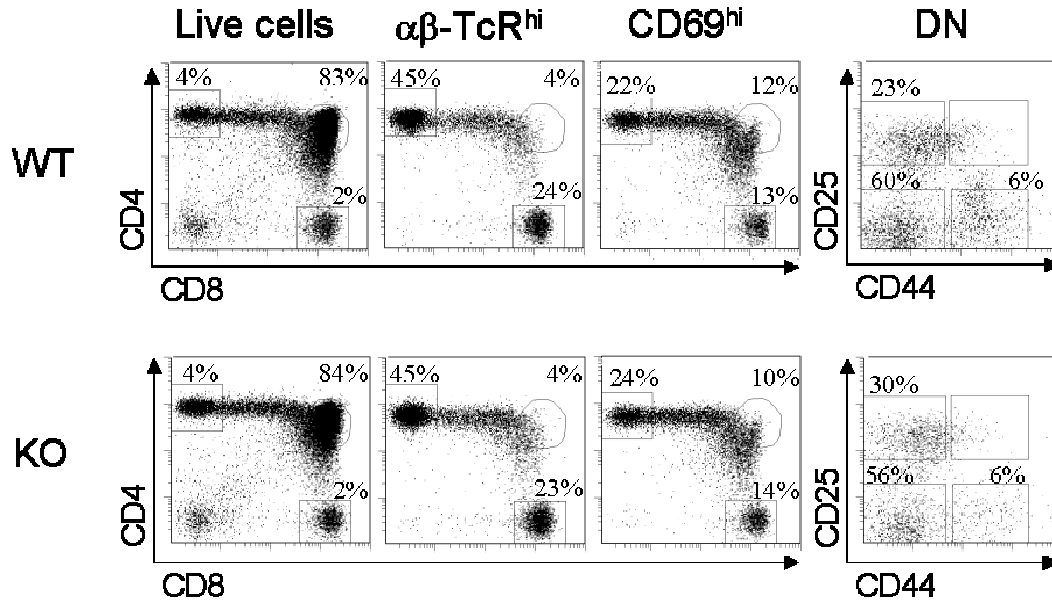
Supporting Figures

Supplemental Figure 1 Legend. (A) The diagram schematizes the relevant *aire* genomic region, with thick exons and thin introns. The targeting vector (middle diagram) contains a *lox* sequence inserted between exons 1 and 2, and the pGK promoter-driven neomycin-resistance gene, flanked by *lox* sequences, introduced between exons 2 and 3. The 7.5 kb NdeI fragment of the targeting construct was electroporated into Sv/129 ES cells. ES clones harboring the homologous recombination event were screened by performing PCR on genomic DNA with primers a and b and then Southern blotting the PCR product with a *lox* oligonucleotide. Further confirmation of homologous recombination was performed by an additional Southern blot (see Materials and Methods). Exhaustive Cre-mediated recombination results in deletion of the second exon of the *aire* gene and the neomycin-resistance cassette (bottom diagram). Cre-mediated excision was performed by genetic crossing of heterozygous mice with CMV-Cre transgenic mice on the C57Bl/6 background. (B) RNA from WT and KO mice was made from thymi and RT-PCR was performed (on two dilutions of RT product) with primers that spanned between exon 1 and exon 4. The PCR products were run on a 2% agarose gel and blotted. The blot was then probed with a labeled oligonucleotide that hybridizes to a region from exon 3. The WT lanes show the expected 545 bp product while the KO lane shows the predicted product size for deletion of exon 2 of 370 bp. (C) The diagram summarizes the splicing of exons 1 to 3 in the KO mouse and the subsequent change in the coding frame. This shift results in a frame-shift and early truncation of the *aire* protein at amino acid 48 (out of 545). The RT-PCR product from the KO lane was also purified and sequenced to confirm the frame-shift.

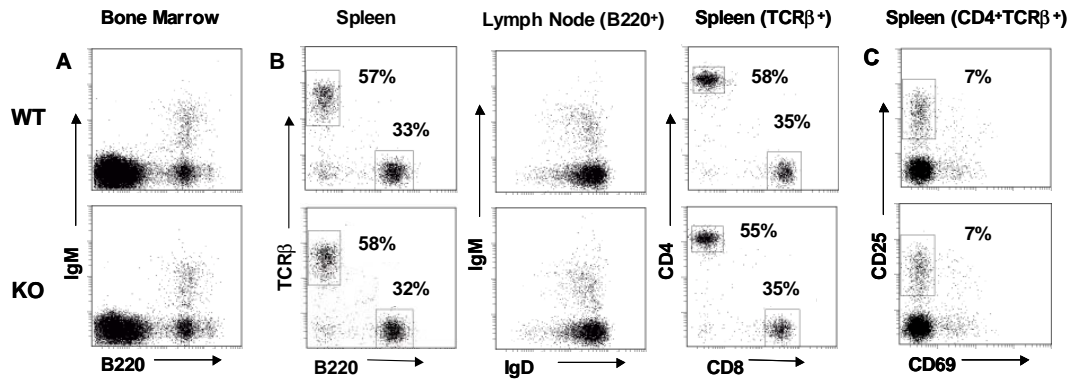
Supplemental Figure 1



Supplemental Figure 2 Legend. Thymocyte immunostaining profiles. Shown are representative plots from individual wild type (upper row) and knockout (lower row) mice. The first three panels are CD4 versus CD8 plots gated on the populations indicated on the upper labels. The far right plot represents CD25 versus CD44 staining for immature thymocytes (DN=CD3-CD4-CD8-B220-CD11b-). Percent cells in the indicated gates are shown on each panel.

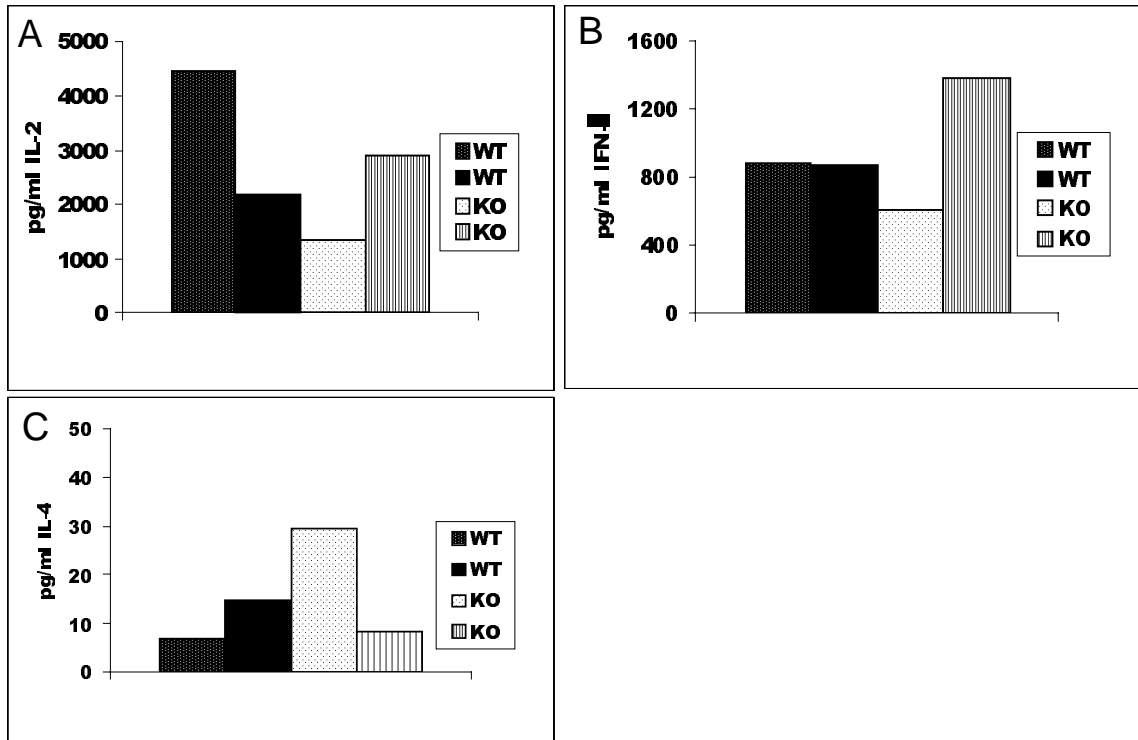
Supplemental Figure S2

Supplemental Figure 3 Legend. Lymphocyte profiles in bone marrow and peripheral lymphoid organs. **(A)** Normal B cell maturation in bone marrow of *aire*^{0/0} mice. **(B)** Normal T- and B-lymphocyte subsets differentiation in the spleens and lymph nodes of *aire*^{0/0} mice. **(C)** CD4⁺CD25⁺ regulatory T cells are not reduced by *aire*-deficiency.

Supplemental Figure 3

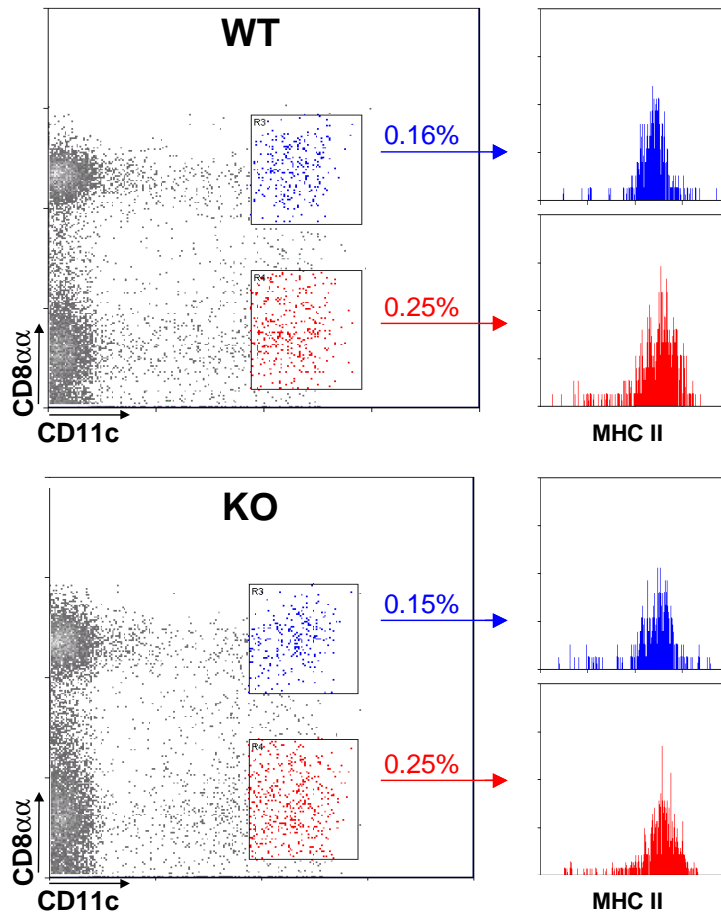
Supplemental Figure 4 Legend. Cytokine production of naïve lymph node cells after stimulation with anti-CD3/anti-CD28. Lymph nodes from two WT and two KO mice of 8 weeks of age were harvested stimulated in vitro with anti-CD3 and anti-CD28. Supernatants were collected at 48 hours post stimulation and assayed for production of IL-2, γ -IFN, and IL-4 by ELISA. **(A)** IL-2 production. **(B)** γ -IFN production. **(C)** IL-4 production. Bars represent values from individual mice. Similar data were generated with spleen cells (11).

Supplemental Figure 4



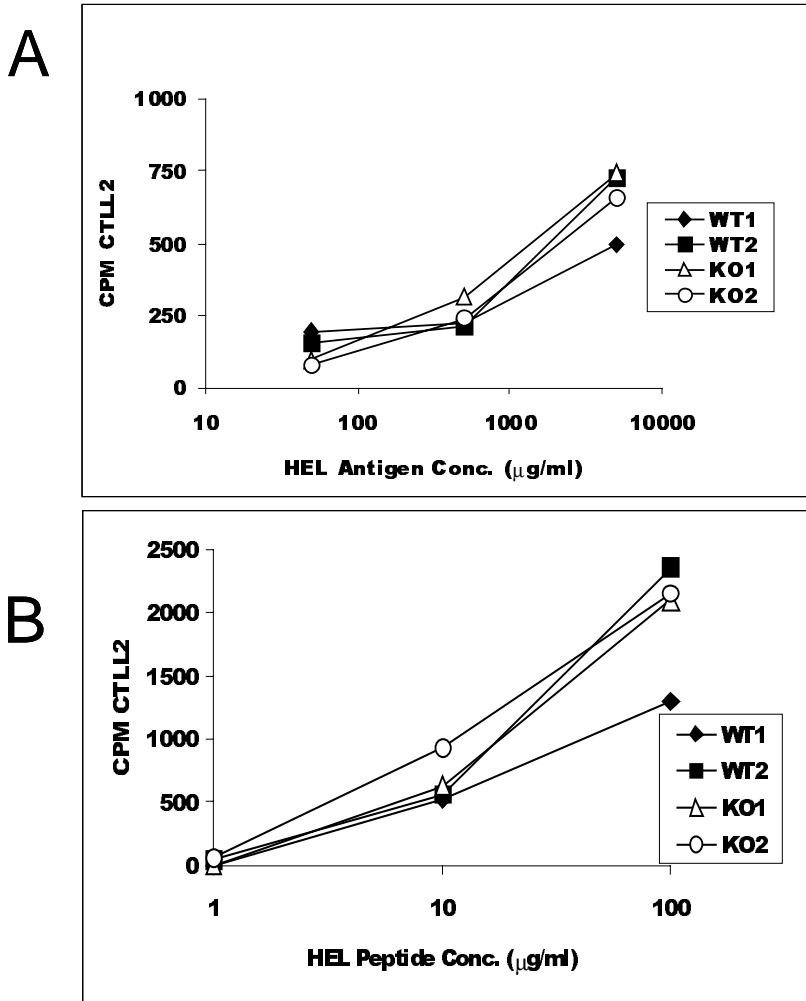
Supplemental Figure 5 Legend. Immunostaining of dendritic cell (DC) subsets in mesenteric lymph nodes from Aire-knockout mice and wild-type littermates. Co-labeling of CD11c (x-axis) and CD8 α (y-axis) on viable, B220⁻ cells. CD8 α ⁺ (blue) and CD8 α ⁻ (red) DC subsets are highlighted in colored boxes. Values represent the percentage of viable cells.

Supplemental Figure 5



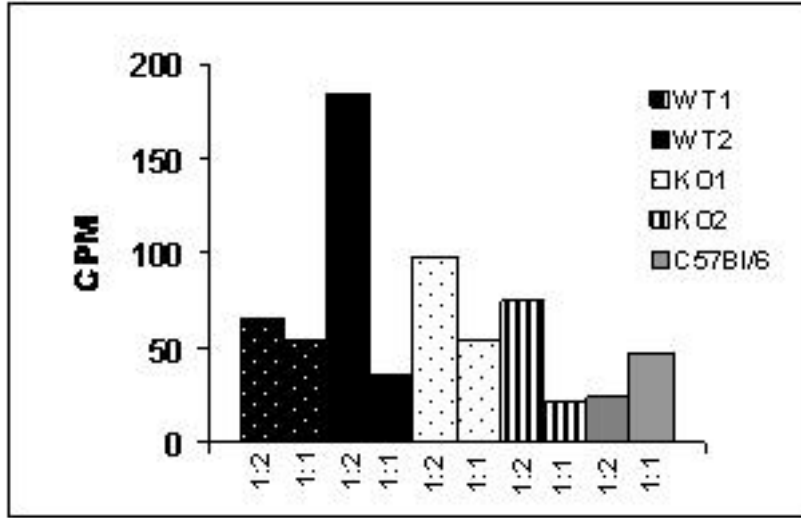
Supplemental Figure 6 Legend. Antigen presentation by splenic cells. Spleen cells were used to present antigen to the T cell hybridoma, B04H91 (specific for HEL 74-96 + I-Ab). Antigen (**A**) or peptide (**B**) was titrated as shown, and IL-2 production measured 24 hours later. Similar results were found for an ovalbumin specific T cell hybridoma, B017.10 (*II*).

Supplemental Figure 6



Supplemental Figure 7 Legend. Mixed lymphocyte reaction (MLR) to self antigen presenting cells (APC's). Splenic cells and inguinal lymph node cells were purified as stimulators and responders, respectively and incubated in a MLR at a 1:2 and a 1:1 ratio of responders:stimulators. Shown are raw CPM of ³H-Thymidine incorporation on day 4 to 5 of responders mixed with self stimulators for 2 knockout, 2 wildtype, and a C57Bl/6 mouse. CPM generated by responders to ConA stimulation were greater than 4000 cpm for all responder groups. The experiment was repeated on three separate occasions, shown is a representative experiment.

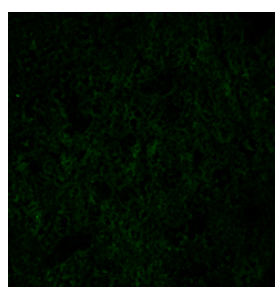
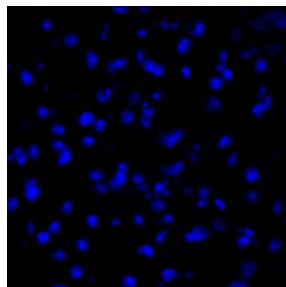
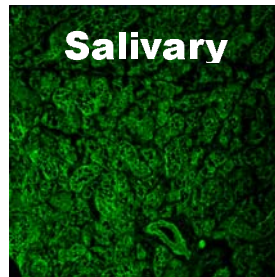
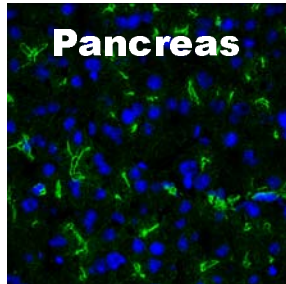
Supplemental Figure 7



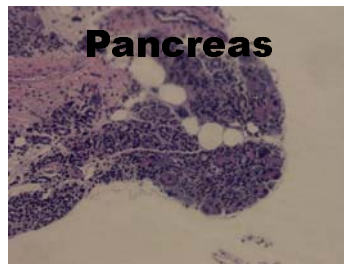
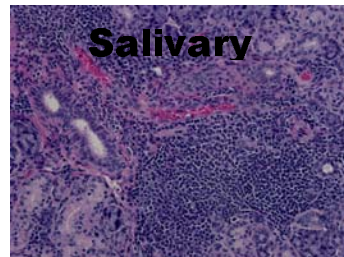
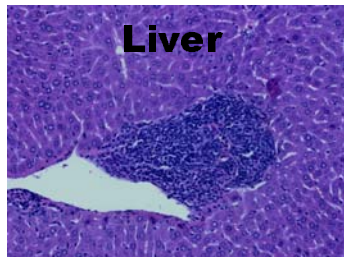
Supplemental Figure 8 Legend. Supplemental histology. **(A)** Autoantibody detection by indirect immunofluorescence with serum from knockout (top row) and wildtype mice (bottom row) for pancreas and salivary gland (250x). Blue represents staining with the nuclear marker DAPI and green represents antibody staining. **(B)** H&E of sections of organs taken from BM chimeras. Liver from a WT>KO mouse showing a lymphoid infiltrate next to a central vein (200x). Salivary from a KO>KO mouse showing diffuse lymphoid infiltrates (200x). Stomach from a WT>KO mouse showing mucosal lymphoid infiltrates (200x). Pancreas from a KO>KO mouse showing marked exocrine pancreatic infiltrates (100x).

Supplemental Figure 8

A



B



Supplemental References

- S1. S. Viville et al., *Cell* **72**, 635 (1993).
- S2. F. Schwenk, U. Baron, K. Rajewsky, *Nucleic Acids Res.* **23**, 5080 (1995).
- S3. D. Vremec and K. Shortman, *J.Immunol.* **159**, 565 (1997).
- S4. J. Derbinski, A. Schulte, B. Kyewski, L. Klein, *Nat Immunol* **2**, 1032 (2001).
- S5. L. M. Green, M. LaBue, J. P. Lazarus, K. K. Colburn, *Lupus* **4**, 187 (1995).
- S6. I. Matsumoto et al., *Nat.Immunol.* **3**, 360 (2002).
- S7. C. Auffray and F. Rougeon, *Eur.J.Biochem.* **107**, 303 (1980).
- S8. J. Rasmussen, A. Goldrath, D. Mathis, C. Benoist, unpublished.
- S9. W. Pan, *Bioinformatics* **18**, 546 (2002).
- S10. V. G. Tusher, R. Tibshirani, G. Chu, *Proc Natl.Acad.Sci U.S.A* **98**, 5116 (2001).
- S11. M. S. Anderson et al., data not shown.